ADVANCED HEALTHCARE MATERIALS
www.advhealthmat.de

# Miniaturized Capsule System Toward Real-Time Electrochemical Detection of $H_2S$ in the Gastrointestinal Tract

*Justin M. Stine, Katie L. Ruland, Luke A. Beardslee, Joshua A. Levy, Hossein Abianeh, Santiago Botasini, Pankaj J. Pasricha, and Reza Ghodssi**

**Hydrogen sulfide ($H_2S$) is a gaseous inflammatory mediator and important signaling molecule for maintaining gastrointestinal (GI) homeostasis. Excess intraluminal $H_2S$ in the GI tract has been implicated in inflammatory bowel disease and neurodegenerative disorders; however, the role of $H_2S$ in disease pathogenesis and progression is unclear. Herein, an electrochemical gas-sensing ingestible capsule is developed to enable real-time, wireless amperometric measurement of $H_2S$ in GI conditions. A gold (Au) three-electrode sensor is modified with a Nafion solid-polymer electrolyte (Nafion-Au) to enhance selectivity toward $H_2S$ in humid environments. The Nafion-Au sensor-integrated capsule shows a linear current response in $H_2S$ concentration ranging from 0.21 to 4.5 ppm ($R^2 = 0.954$) with a normalized sensitivity of 12.4% $ppm^{-1}$ when evaluated in a benchtop setting. The sensor proves highly selective toward $H_2S$ in the presence of known interferent gases, such as hydrogen ($H_2$), with a selectivity ratio of $H_2S$:$H_2 = 1340$, as well as toward methane ($CH_4$) and carbon dioxide ($CO_2$). The packaged capsule demonstrates reliable wireless communication through abdominal tissue analogues, comparable to GI dielectric properties. Also, an assessment of sensor drift and threshold-based notification is investigated, showing potential for in vivo application. Thus, the developed $H_2S$ capsule platform provides an analytical tool to uncover the complex biology-modulating effects of intraluminal $H_2S$.**

## 1. Introduction

Inflammatory bowel disease (IBD) is characterized by chronic inflammation of intestinal tissues and can be associated with dysbiosis of the gut microbiome.[1] Although altered gut bacterial composition has been linked with gastrointestinal (GI) conditions including colorectal cancer (CRC), ulcerative colitis (UC), irritable bowel syndrome (IBS), and metabolic diseases, the physiologic link between dysbiosis and observed pathology has yet to be discovered.[2–5] Moreover, many digestive diseases share vague and overlapping symptoms such as abdominal pain, nausea, and diarrhea, posing a challenge in delivering a timely diagnosis.[6,7] Current techniques to diagnose GI disorders in the GI tract rely on endoscopic techniques (e.g., upper endoscopy and colonoscopy) for visualizing and sampling the lumen. More recently, capsule endoscopy has emerged as a noninvasive alternative to traditional endoscopy, capable of accessing distal regions of the small intestines (e.g., jejunum and ileum) and other elusive areas to

J. M. Stine, K. L. Ruland, H. Abianeh, R. Ghodssi
Department of Electrical and Computer Engineering
University of Maryland
College Park, MD 20742, USA
E-mail: ghodssi@umd.edu

The ORCID identification number(s) for the author(s) of this article can be found under https://doi.org/10.1002/adhm.202302897



**DOI: 10.1002/adhm.202302897**

J. M. Stine, K. L. Ruland, L. A. Beardslee, J. A. Levy, S. Botasini, R. Ghodssi
Institute for Systems Research
University of Maryland
College Park, MD 20742, USA

J. M. Stine, K. L. Ruland, J. A. Levy, R. Ghodssi
Fischell Institute for Biomedical Devices
University of Maryland
College Park, MD 20742, USA

J. A. Levy, R. Ghodssi
Department of Materials Science and Engineering
University of Maryland
College Park, MD 20742, USA

P. J. Pasricha
Department of Internal Medicine
Mayo Clinic Hospital
Phoenix, AZ 85054, USA

detect morphological indicators of GI disorders. Previously published and commercialized GI tract sensing platforms employ a variety of sensing technologies including acoustic and optical imaging, as well as physiological readings (e.g., pH, pressure, temperature); however, these modalities fail to detect specific molecular biomarkers of microscopic disease.[8] To better understand the association between microbial activity, inflammation, and disease pathology, sensors that target molecular analytes of interest and in situ technologies enabling their deployment are required.

Intraluminal gases have been identified as biomarkers of bacterial diversity and overall gut health. These gases diffuse from the bloodstream to the GI tract or can be released as byproducts of intestinal microbiota.[9] The concentration, type, and volume of intestinal gas can serve as an indicator of chronic GI conditions. For instance, elevated hydrogen ($H_2$) and methane ($CH_4$) levels in the breath may suggest lactose intolerance, carbohydrate maldigestion and malabsorption syndromes, and small intestinal bacterial overgrowth (SIBO).[10,11] Hydrogen sulfide ($H_2S$) is one of three gasotransmitters in the GI tract and has received significant attention as an endogenous mediator of inflammation, mucosal repair, and homeostasis.[12] Endogenous $H_2S$ is produced enzymatically (from L-cysteine substrates) in tissues throughout the body, while exogenous $H_2S$ is produced by intestinal microbiota, such as sulfate-reducing bacteria (SRB).[13] Depending on the local concentration, source, and bioavailability, $H_2S$ is believed to contribute to both pro- and anti-inflammatory mechanisms.[14,15] In excess, $H_2S$ can inhibit oxidation and destabilize mucus layers protecting the epithelium, and has been observed at elevated levels in numerous diseases, including IBD, CRC, obesity, halitosis, pouchitis, and periodontitis.[16] In contrast, low concentrations of $H_2S$ can invoke therapeutic effects, supporting mucus layer reconstitution and resolving tissue injury and inflammation.[17] Therefore, monitoring $H_2S$ levels in the GI tract would provide insight into how microbial gas production influences gastrointestinal physiology and its relation to disease pathogenesis.

Breath testing, analysis of flatus and fecal samples, and endoscopic collection are currently standardized methods for quantifying gut microbial $H_2S$ production indirectly; however, noninvasive, real-time solutions are lacking.[10,11] Unlike $H_2$ and $CH_4$, $H_2S$ has a short circulating half-life due to active detoxification and high chemical reactivity, preventing relevant concentrations of intestinal $H_2S$ from reaching the breath. Moreover, $H_2S$ produced by oral microbes (e.g., halitosis) can interfere with breath measurements, further complicating the assessment of the $H_2S$-producing metabolism.[18] Previous clinical studies have successfully quantified $H_2S$ concentrations in the colon from flatus and fecal analysis (0.2–30 parts per million [ppm]), forming definitive associations between the production of $H_2S$, microbial composition, and diet.[19,20] However, these methods lack the temporal and spatial resolution required to accurately represent the current state of the intestines. Notably, they obscure key $H_2S$ information in the small bowel, and as a result, precise $H_2S$ concentration levels are unknown. Fully controllable, miniaturized systems capable of real-time, onsite detection of short-lived bacteria-derived inflammatory markers are critically needed for improved disease management.

Recent advances in flexible electronics, chemical sensors, and smart packaging have contributed to the emergence of ingestible capsule technologies capable of monitoring gaseous molecules in the gut.[21–25] In general, ingestible gas sensors must operate in both aerobic and anaerobic environments, withstand moisture and caustic conditions, and minimize interference from other electroactive molecules.[26] Kalantar-zadeh et al. and others have demonstrated wireless ingestible capsules equipped with metal-oxide field effect transistor (FET) sensors capable of monitoring oxygen ($O_2$), $H_2$, and $CO_2$ levels in the GI tract.[21] Studies were performed to assess microbiota fermentation processes in response to dietary intervention and exploit the progressively anaerobic conditions in the small and large intestines to track the capsule's position. Metal-oxide FET sensors detect changes in resistance upon adsorption of the target gas and manipulate temperature to modulate selectivity. This method, unfortunately, is not selective enough to sense trace gases, such as nitric oxide (NO) and $H_2S$, which are not easily distinguished from predominant gaseous species in the GI tract (e.g., $H_2$ and $CH_4$). Alternatively, electrochemical sensing offers a low-power, real-time, and scalable sensing modality suitable for detecting NO and $H_2S$; however, few ingestible capsule devices possess electrochemical sensing capabilities, and none are capable of selectively detecting $H_2S$ in the GI tract.[27,28] Implantable electrochemical sensing modules have successfully detected dynamic changes of NO in response to induced inflammation, though integration into a capsule embodiment has yet to be realized.[29–31] Commercial screen-printed $H_2S$ sensors, such as the 3SP-H2S-50 (SPEC Sensors LLC, Irvine, CA), offer a potential path toward system miniaturization.[32] We successfully detected $H_2S$ at room temperature (at 0 V-bias) using a previous ingestible capsule configuration, which integrated a 3SP-H2S-50 with a miniature sensor package.[33] It was found that the modified carbon electrodes were inoperable under humid conditions, had insufficient operational lifetime, and lacked selectivity toward $H_2$, making them incompatible for embedded gas sensing applications.

To address these challenges, here, we report a fully integrated gas-sensing ingestible capsule for real-time, wireless detection of $H_2S$ in the GI tract (**Figure 1A**). The system, as shown in Figure 1B, features a thin, flexible electrochemical sensor utilizing a Nafion solid-state polymer electrolyte (SPE) and gold (Au) sensing electrode (Nafion-Au) to selectively monitor physiological $H_2S$ concentrations. The capsule electronics integrate an electrochemical analog front-end (AFE) to facilitate amperometric measurements and a Bluetooth Low Energy microcontroller (BLE-MCU) for data processing and wireless transmission. The components are mounted on a flex-rigid printed circuit board (PCB) and encapsulated in a soft polydimethylsiloxane (PDMS) polymer. A 3D-printed spacer unit was placed between the PCB to allow for integration of future system modalities, resulting in an overall capsule form factor of $14 \times 34$ mm$^2$. This size and shape are compatible with large porcine animal models and can be readily scaled for implementation in vivo. Pretreatment of the Nafion SPE to increase the conductivity and hydration capacity of the membrane was investigated. The operability of the ingestible capsule prototype was evaluated in a custom humidity-controlled gas testing chamber. Electrochemical characterization demonstrated linear detection of $H_2S$ over concentrations ranging from 0.21 to

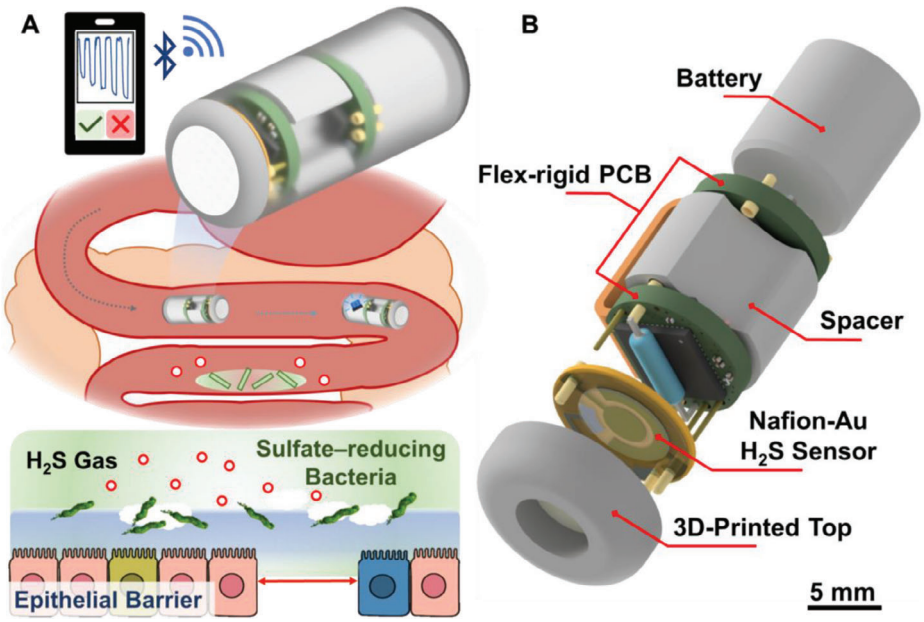


**Figure 1.** Conceptual overview of the wireless gas-sensing capsule platform. A) Schematic representation of the amperometric gas-sensing capsule monitoring the exogenous production of $H_2S$ from SRB in the gastrointestinal tract and wirelessly transmitting data to an external phone. B) CAD rendering showing an exploded view of the ingestible capsule, including a flex-rigid PCB, 3D-printed spacer and sensor top, Nafion-Au $H_2S$ sensor, and 3 V coin cell battery.

4.5 ppm (14.6 μM) and excellent selectivity to $H_2S$ in the presence of 100-fold greater concentrations of interfering gases, namely $H_2$, carbon dioxide ($CO_2$), and $CH_4$. This device addresses system integration challenges associated with amperometric detection of $H_2S$ in the GI tract and proves capable of identifying fluctuations of $H_2S$ levels under simulated GI environment conditions. Such a device can provide new insights into the complex immune-modulating effects of intraluminal $H_2S$ and its role in disease pathogenesis, unlocking its potential as an inflammatory biomarker for disease treatment and monitoring.

## 2. Results and Discussion

### 2.1. $H_2S$ Sensing Mechanisms

Electrochemical detection of $H_2S$ has been previously demonstrated.[34–36] However, these sensors are often incompatible with the intraluminal environment, and lack the selectivity, sensitivity, and low-voltage operation essential for integration with ingestible capsule platforms. Electrode materials like platinum and modified carbon that are sensitive to $H_2S$ due to their affinity to $H_2$, do not provide the necessary selectivity for intestinal $H_2S$ sensing, as $O_2$, nitrogen ($N_2$), $CH_4$, $CO_2$, and $H_2$ (up to 50%) make up 99% of intestinal gas.[37] Au is sensitive to $H_2S$ via a high adsorption affinity to sulfur molecules, and is not reactive to $H_2$.[38] Mubeen et al. utilized this sensing mechanism to develop an $H_2S$ sensor employing single-walled carbon nanotubes (SWNT) decorated with Au nanoparticles.[39] However, the sensor required a bias voltage ranging from 1–4 V for the desorption of sulfur (S) from the Au electrode, resulting in a slow response and recovery time. When Au is exposed to $H_2S$, sulfur atoms covalently bond with the Au surface. Au—S covalent bonds significantly reduce the work function of Au and require a substantial amount of energy to reverse. Therefore, while Au alone can be used to sense $H_2S$, further modification of the working electrode is necessary to achieve the sensitivity and recovery characteristics to sense trace concentrations of intraluminal $H_2S$ gas in real-time.

The electrochemical $H_2S$ sensor (Ø = 12 mm) in this work is comprised of a thin-film Au working electrode (WE, Ø = 4 mm), Au counter electrode (CE), and a silver (Ag) reference electrode (RE) evaporated on a flexible polyimide substrate (Kapton, 1 mil) (**Figure** 2A-i). Laser-cut acrylic wells were then attached to the sensor to serve as a reservoir for forming the Nafion membrane from dispersion. To integrate the sensor with the capsule electronics, Au pins were connected to each electrode contact pad using Ag epoxy (Figure 2A-ii). Then, 5% w $v^{-1}$ Nafion dispersion (EW, 1100 g $eq^{-1}$) was drop-cast into the acrylic reservoir to sufficiently cover the entire sensor area (Ø = 6 mm), followed by subsequent pretreatment with sulfuric acid ($H_2SO_4$), as shown in Figure 2A-iii. Finally, a Teflon membrane (Ø = 6 mm, pore size: 5 μm) was lightly pressed into contact with the treated Nafion film and sealed (Figure 2A-iv). The Teflon membrane functions as a gas-permeable, liquid-impermeable interface between the Nafion and the external environment, limiting sensor corrosion and fouling.

Nafion is a chemical-resistant perfluorinated cationic-exchange polymer (CEP) with exceptional membrane-forming capabilities and is often used as an SPE to enhance the sensitivity, conductivity, and recovery of the fabricated sensor. Dispersion and baking of Nafion crosslinks the polytetrafluoroethylene (PTFE) backbone to form stable clusters of hydrophilic sulfonic acid end groups surrounded by hydrophobic PTFE. The hydrophilic regions expand as the membrane is hydrated and connect into a network of ionic conduction channels if sufficiently hydrated. Water uptake, ion exchange capacity, and ion

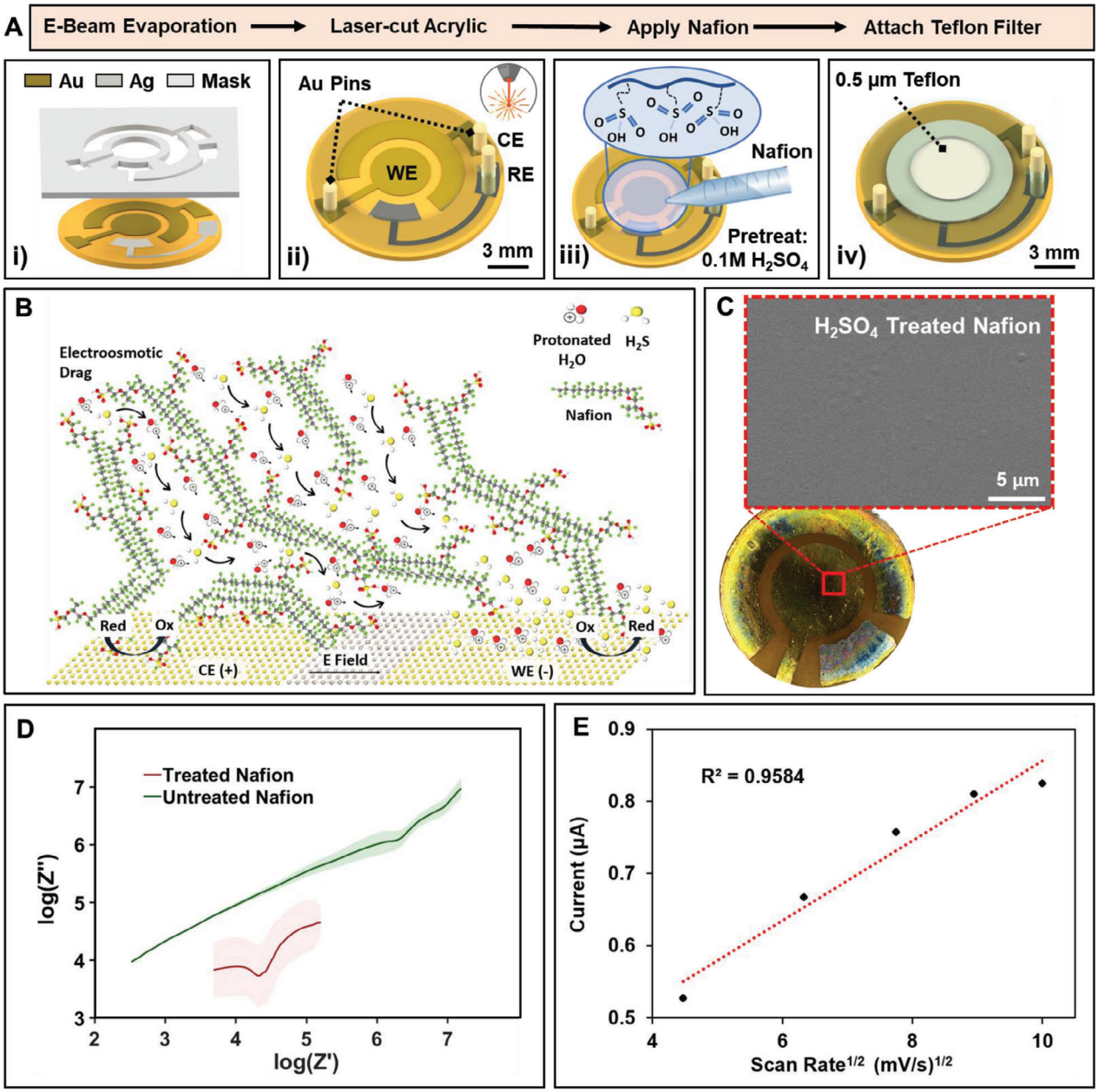


**Figure 2.** Design and evaluation of Nafion-Au $H_2S$ sensor. A) Fabrication and assembly process of the microfabricated $H_2S$. (i) Metal layers are patterned onto a flexible Kapton film using a paper mask. (ii) Laser-cut acrylic wells were adhered to create an electrolyte reservoir and align Au contacts for connecting the sensor with the capsule electronics. (iii) Nafion dispersion was drop-cast on the sensor and dried for 24 h, followed by pretreatment with $H_2SO_4$ for 48 h, then rinsed and hydrated using DI water. (iv) The Nafion film was sealed with a 0.5 µm pore Teflon membrane and additional acrylic well. B) Schematic of electroosmotic drag of $H_2S$ via electroosmotic flow of the positively charged water molecules in hydrated Nafion due to an electric field between the CE and WE. The accumulation of protonated water molecules and $H_2S$ at the WE increases the rate of reduction, thereby increasing negative current flow. C) SEM image of the Nafion coated sensor showing a uniform membrane free of cracks. D) Nyquist log–log plot comparing the average EIS ($N = 3$) of the sensors before acid treatment (green) and after 48 h acid treatment (red) with 0.1 M $H_2SO_4$. E) Current versus Scan Rate$^{1/2}$ for CV applied to sensor with 2.3 ppm of $H_2S$ present for 20–100 mV $s^{-1}$ scan rate at 20 mV $s^{-1}$ intervals. Current response at −0.2 V bias voltage was taken as the reduction peak. Error bars shown as shaded regions of standard deviation (SD) of mean.

conductivity together determine the conductivity of the Nafion membrane.[40–44] While this hydration dependence is problematic for some applications, the high-water content of the GI tract is expected to provide sufficient humidity levels to hydrate the Nafion and ensure conductivity throughout capsule transit. When a hydrated CEP is biased, protonated water molecules (e.g., $H_5O_2^+$, $H_9O_4^+$) flow from the anode to the cathode of the sensor, simultaneously transporting $H_2S$ and other small gaseous molecules in the process, as illustrated in Figure 2B. This electroosmotic drag results in an accumulation of $H_2S$ molecules and protons at the surface of the WE, reducing the work function of Au and increasing the reduction current.[45–50]

Investigators have demonstrated that Nafion membrane conductivity increases with decreasing thickness until reaching the thin-film regime (<10 µm).[51,52] To achieve a uniform Nafion membrane at the desired thickness, removal of the solvent and surface interactions between the Nafion dispersion and Au substrate are critically important. Slowly evaporating the Nafion dispersion allows for an even distribution of hydrophilic and hydrophobic regions in the Nafion, resulting in higher conductivity.[41,53] Therefore, the rate of solvent evaporation was carefully controlled in order to minimize the risk of cracks forming in the film.[54] To accomplish this, we introduced additional solvent (80% ethanol) into the sealed container and allowed it to evaporate for 24 h.[51] The Nafion-Au sensors were then baked in a furnace at 80 °C for 1 h to remove any remaining solvent subsequently placed in a sealed humid container for 24 h to rehydrate.

To enhance water uptake and increase conductivity, Nafion is often protonated through pretreatment with strong acids (e.g., nitric acid ($HNO_3$), hydrochloric acid (HCl), $H_2SO_4$, and phosphoric acid ($H_3PO_4$)) having p$K_a$ values less than 1 p$K_a$. During this process, hydrogen ions ($H^+$) from the acid are donated to the sulfonic acid end groups in Nafion. Several groups have investigated the efficacy of Nafion pretreatment by varying acid type, concentration, temperature, and treatment time, then evaluating the resulting membrane under various humidity values and temperatures.[48,55,56] Overall, the Nafion pretreatment resulted in improved conductivity and water uptake for sensors treated with acids of similar or higher p$K_a$ values than Nafion (≈−6 p$K_a$). Kuwertz et al. found that $H_2SO_4$ (−10 p$K_a$) exhibited the highest conductivity and water uptake in sensing environments with humidity levels between 80% and 100%,[56] closely resembling the conditions of the GI tract. Therefore, the Au-Nafion sensor presented in this work was protonated with $H_2SO_4$.

To identify a suitable pretreatment procedure for protonation of the Nafion coated Au electrodes, varied concentrations of $H_2SO_4$, treatment time intervals, and solution temperatures were investigated. Preliminary amperometric measurements were recorded for each combination of $H_2SO_4$ in Figure S1 (Supporting Information). While sensors treated with 1.0 M $H_2SO_4$ exhibited higher linearity and a consistent bias voltage, they displayed low conductivity and poor sensor durability regardless of test conditions. This outcome was likely due to a combination of insufficient acid protonation time and corrosion of the Cr seed layer beneath the Au WE and Ag RE, leading to reduced electroactive surface area.[57,58] When testing various protonation times for 0.1 M $H_2SO_4$, a protonation time of 24 h or less resulted in low membrane conductivity. In contrast, a 48 h protonation time produced stable, conductive sensors without corrosion of the Cr seed layer. Therefore, the Au-Nafion sensors were treated by dispersing 0.1 M $H_2SO_4$ (50 µL) and resealing the sensor in a humid container for 48 h to allow the acid to protonate the film, followed by rinsing with deionized (DI) water. This resulted in an evenly dispersed Nafion membrane that demonstrated consistent conductivity and mechanical durability once baked and treated, providing a final film thickness of ≈45 µm. Inspection of the WE via a scanning electron microscope (SEM), Phenom XL (Nanoscience Instruments, Alexandria, VA), confirms a uniform membrane without cracks or deformities in the Nafion or electrode which would impact conductivity and sensor durability (Figure 2C). Electrical impedance spectroscopy (EIS) was utilized to characterize the Nafion-coated sensors. Figure 2D shows the average impedance of the Nafion-Au sensor before and after acid treatment, confirming significant improvement in the membrane conductivity. While the acid pretreatment is not expected to impact shelf life, it is important to store protonated Nafion membranes in environments without fluctuations in humidity. The sensors were stored at room temperature in a dry environment away from direct sunlight until use.[59,60] As a result, the sensors were able to retain conductivity for over 12 h of testing.

### 2.2. Benchtop Characterization of Nafion-Au $H_2S$ Sensor

The electrochemical response of the fabricated $H_2S$ gas sensor was evaluated using a benchtop potentiostat (CHI660D, CH Instruments Inc) and custom gas-testing setup, as described in Figure S2 (Supporting Information). Specific gas concentrations of various intraluminal gas species were achieved by controllably venting gas into a plastic test chamber (2400 mL)—diluted with air—until the desired concentration was reached. Gas concentration was calculated using Equation (1) with gas-testing setup and infill parameters summarized in Table S1 (Supporting Information). To preserve the conductivity of the Nafion membranes, all experiments were performed under humid conditions. This was achieved by periodically venting water vapor into the chamber for 60 s along with the gaseous analytes. Cyclic voltammetry (CV) was applied in the potential range of +0.2 and −0.2 V (scan rate: 100 mV $s^{-1}$) to observe cathodic currents. Figure S3 (Supporting Information) presents the cyclic voltammogram of the fabricated Nafion-coated $H_2S$ sensors at different gas saturation states: ambient air, 2.3 and 4.5 ppm of $H_2S$. An increasingly negative reduction current response corresponding with increased $H_2S$ concentration was observed between −0.1 and −0.2 V (vs Ag), indicating a range of suitable bias voltages to detect $H_2S$. Therefore, subsequent amperometric measurements were performed at a bias voltage of −0.2 V to maximize the sensitivity of the Nafion-Au sensor to $H_2S$, while avoiding potential interference from reduction peaks of $O_2$. The influence of scan rate on the sensor response to $H_2S$ was also examined by comparing cyclic voltammograms of different scan rates when the sensor was exposed to 2.3 ppm of $H_2S$ (Figure 2E). The results demonstrated that the current response corresponded to changes in $H_2S$ gas, and that the system was diffusion controlled (linear relationship between current and the square-root of scan rate). The CV waveforms for each scan rate are summarized in Figure S4 (Supporting Information).

To generate a calibration curve for the $H_2S$ sensor, we introduced concentrations ranging from 0.9 to 4.5 ppm of $H_2S$ into the custom gas chamber at 0.9 ppm intervals (refer to Table S1 (Supporting Information) for infill time calculations) following a 10 min warm-up time. Electrochemical sensors typically require a brief warm-up time to allow the electrodes and electrolyte to equilibrate under a voltage bias. Negligible differences in sensor readout due to changes in temperature when operating either at ambient (22 °C) or internal body temperatures (37 °C) were observed, thus all experiments were conducted at room temperature. As the sensor is intended to continuously measure $H_2S$, the voltage bias will be applied at least 10 min before ingestion. The amperogram of a single sensor is shown in **Figure 3**A, where increasing

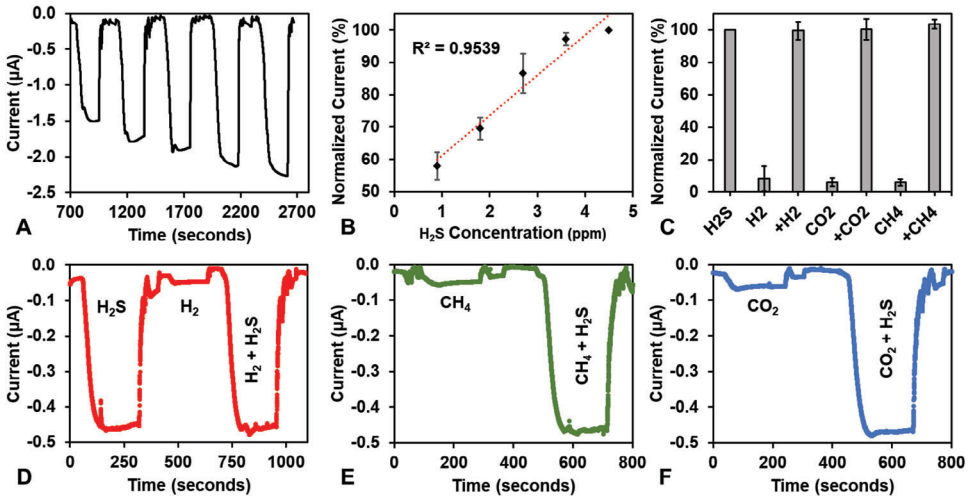


**Figure 3.** Benchtop characterization of $H_2S$ sensor. A) Amperogram showing the current response of the Nafion-Au sensor for increasing $H_2S$ concentrations at 0.9 ppm intervals (range: 0.9–4.5 ppm) and B) the resulting calibration curve normalized to the current response at 4.5 ppm (set to 100%) for each sensor ($N = 3$). C) Selectivity of $H_2S$ against known interferent gases $H_2$ (500 ppm), $CH_4$ (415 ppm), and $CO_2$ (16 650 ppm) was evaluated, and the normalized current response was compared ($N = 3$). Selectivity waveforms depicting the current response for concentration ratios of D) $H_2S$:$H_2$ = 110.8, E) $H_2S$:$CO_2$ = 3688.6, and F) $H_2S$:$CH_4$ = 92.8, resulting in current response ratios [$H_2S$:interferent gas] of $H_2S$:$H_2$ = 12.2, $H_2S$:$CO_2$ = 16.8, and $H_2S$:$CH_4$ = 16.6. Error bars shown as standard deviation (SD) of mean.

and decreasing sensor current output reflects both an increase and decrease in $H_2S$ concentration. After $H_2S$ was vented into the chamber, the current increased rapidly until reaching saturation after 3 min (including infill time). To return the chamber to an ambient baseline condition (air), the chamber contents were removed using a vacuum pump. The required time to return the sensor to its baseline value was dependent on the gas concentration in the chamber, though purging for three 20 s pulses with a 15 s pause between them was sufficient for all test values and preserved the sensor's lifetime. The resulting calibration curve, shown in Figure 3B, depicts the normalized average current response from multiple Nafion-Au $H_2S$ sensors ($N = 3$), where 100% represents 4.5 ppm $H_2S$. A linear current response (correlation coefficient $R^2 = 0.954$) and sensitivity of 12.4% $ppm^{-1}$ was observed with slight current saturation starting at 3.5 ppm. At 5.4 ppm, there was no discernable difference between an increase in $H_2S$ and noise (Figure S5, Supporting Information). Differences in the current response, shown by Figure 3B error bars, can be attributed to slight variations in Nafion membrane thickness, hydration, and the density of Nafion clusters in the membrane. As calibration of Nafion-based sensors is highly humidity dependent, the $H_2S$ sensors were calibrated in ≈100% humidity, based on the expected humidity of the GI tract.[61]

We characterized the selectivity of the Nafion-Au sensor between $H_2S$ and potential interferent gases in the GI tract. Amperometric measurements of 4.5 ppm $H_2S$ were performed in the absence and presence of 415 ppm $CH_4$, 16 650 ppm $CO_2$, and 500 ppm $H_2$, respectively. The resulting amperograms demonstrated that accurate detection of $H_2S$ remained mostly unaffected in the presence of greater than 100-fold concentrations of $CH_4$, $CO_2$, and $H_2$ (Figure 3C). Figure 3D–F shows the sensor response for each gas and indicate less than 10% variation when comparing the combined signal response from $H_2S$ and interferent gases to the $H_2S$ baseline. Overall, the fabricated $H_2S$ sensor demonstrated selectivity to $H_2S$ in the presence of all interferent gases, including $H_2$, and outperformed the commercial 3SP-H2S-50 SPEC-H2S sensor which showed elevated current response to $H_2$ (Figure S6, Supporting Information).

### 2.3. Ingestible Gas-Sensing Capsule Design

Miniaturized potentiostat electronics (Ø = 12 mm) capable of performing amperometric measurements were developed, as shown in Figure S7A (Supporting Information), to facilitate in situ sensing using the Nafion-Au $H_2S$ sensor. The system incorporates several commercial off-the-shelf (COTS) components (operated at 3.3 V): 1) an electrochemical AFE, AD5941 (Analog Devices, Wilmington, MA), to excite the electrochemical sensor and record resulting current values, 2) a BLE-MCU, BGM13S (Silicon Labs, Austin, TX), and external 2.45 GHz ceramic chip antenna, WLA.01 (Taoglas, San Diego, CA), for wireless data acquisition, and 3) a 3.0 V, 160 mA h lithium manganese dioxide ($LiMnO_2$) coin-cell battery (Ø = 11.6), 2L76 (Energizer, St. Louis, MO), and magnetic reed switch to shut off the device when not in use (Figure S7B, Supporting Information). Inter-device communication is handled by a serial peripheral interface (SPI) for system configuration and to facilitate data transfer between the AFE and BLE-MCU (Figure S7C, Supporting Information). The BLE-MCU was programmed to receive and transmit data wirelessly via BLE using the EFR Connect phone app (Silicon Labs, Austin, TX) and a custom GATT profile. This allowed for remote calibration and initiation of amperometry gas measurements, as well as control of the energy modes of the on-board electronics.

When an amperometric measurement is initiated, the AFE applies a bias voltage across the WE and RE. The resulting current response between the CE and WE is passed through a transimpedance amplifier (TIA), where the signal is converted to a voltage and amplified. Data are sampled every 100 ms and digitized via an internal analog to digital converter (ADC), then stored

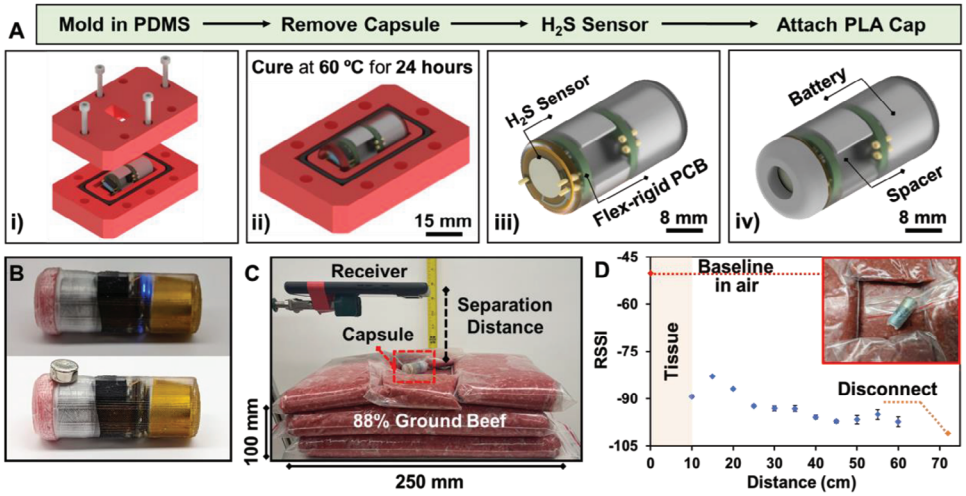


**Figure 4.** Packaging and characterization of capsule electronics. A) Molding and assembly process of the $H_2S$ gas sensing capsule. (i) Capsule components are sealed into 3D-printed mold and encapsulated in PDMS. (ii) After the PDMS is cured for 24 h, the capsule is released. (iii) The $H_2S$ sensor is attached to the exposed Au pins of the PCB and (iv) a PLA cap with a sealed Teflon filter is epoxied to protect the $H_2S$ gas sensor. B) Photograph of packaged gas-sensing capsule demonstrating the on (blue light) and off state using a neodymium magnet to trigger the magnetic reed switch. C) Wireless signal attenuation setup depicting the capsule prior to being surrounded on each side by 100 mm of ground beef (88% Lean, 12% Fat) with the receiver (phone) placed directly above it. D) Bluetooth attenuation was recorded between the smart phone (sensitivity = −101 dBm) and packaged capsule system (system baseline = −52 dBm) at a 50 mm interval until measurement failure. Data points represent the averaged RSSI value collected from ≈30 data packets, showing sustained communication until 720 mm. Error bars shown as standard deviation (SD) of mean.

temporarily to a ferroelectric random-access memory (FRAM) onboard the AFE. Simultaneously, the BLE-MCU periodically interrogates the status of the FRAM (100 ms interval) to determine whether data are available for wireless transmission to the phone. In this active transmission mode, the device consumes an instantaneous current of 10 mA and average of 3.5 mA. Battery life-time calculations estimate a 29 h capsule lifetime under continuous operation of the wireless communication and amperometric gas sensor. While the capsule size and form factor presented here is larger than existing FDA-approved ingestible electronics,[62] the current dimensions are acceptable for in vivo large porcine models. Ingestible capsules of varied size and function, employed in vivo for testing in porcine studies, are summarized in Table S2 (Supporting Information).[25,63–73] The main limiting factors for further scaling the $H_2S$ sensing capsule are the size of the COTS electronic components and compatibility of the battery chemistry. Bluetooth LE has an instantaneous current consumption of ≈10 mA (at +0 dB antenna gain), which prevents the use of alternative safe battery chemistries, such as silver oxide (Ø = 9.5 mm), without greatly reducing the wireless transmission rate (10 s).[74] Future work will focus on sourcing alternative electronic components with smaller device footprints (e.g., AD5940), as well as optimize the data acquisition rate to minimize power consumption, allowing access to smaller coin cell batteries. The gas-sensing capsule electronics were validated using commercial screen-printed $H_2S$ sensors (3SP-H2S-50) prior to packaging, as shown in Figure S8 (Supporting Information).

### 2.4. Characterization of the Packaged Gas-Sensing Capsule

The benchtop validated sensor was integrated with the capsule electronics and packaged in two stages: 1) encapsulation of the electronic components in a soft polymer and 2) attachment and sealing of the $H_2S$ sensor to preserve the hydration of the Nafion SEP during subsequent evaluation of the packaged device. Here, capsule electronics were encapsulated in PDMS at a 10:1 monomer to curing agent ratio and baked at 65 °C for 24 h prior to removal (**Figure** 4A-i). PDMS encapsulation is straightforward, repeatable via molding, resilient to acidic environments, and biocompatible.[75] While there are concerns regarding the potential for liquid uptake through PDMS molds, modified curing parameters and additional coating of Parylene C have been shown to minimize this effect.[76,77] The packaged capsule has a resulting 14 × 34 $mm^2$ cylindrical form factor (Figure 4A-ii). Figure 4A-iii shows the modular attachment of the $H_2S$ sensor and molded capsule electronics. Finally, a 3D-printed cap (Ø = 14 mm) made from polylactic acid (PLA) was sealed to the PDMS capsule with a biocompatible epoxy to cover the Teflon protected sensor while still allowing gas to diffuse from the external environment (Figure 4A-iv). When not in use, the capsule system was placed on an external magnet to disconnect the battery via the magnetic reed switch. This is demonstrated in Figure 4B, where a small neodymium magnet (1 $cm^2$, ≈600 mT) placed less than 20 mm distance from the magnet reed switch is sufficient to disconnect the system as indicated by the blue light emitting diode (LED).

### 2.5. Bluetooth Characterization for Ingestible Operation

Wireless medical devices, including ingestible capsules, wearable sensors, and implantable devices typically operate within the 405, 915 MHz, and 2.45 GHz ISM frequency bands. Bluetooth, which operates at 2.45 GHz, is a low-power, point-to-point communication protocol that permits a compact antenna footprint and is

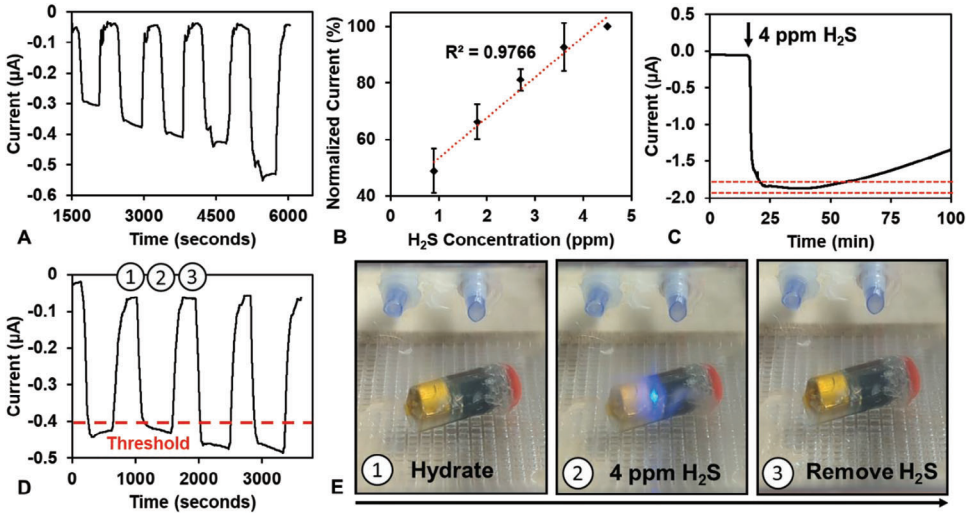


**Figure 5.** Electrochemical characterization of the ingestible capsule prototype. A) Wireless amperometric measurement of $H_2S$ with the sensor-integrated capsule and B) the resulting calibration curve. C) A drift measurement was conducted following a 10 min warm-up time at 3.6 ppm $H_2S$ concentration. A linear sensor drift (+0.1 nA $s^{-1}$) was observed after 30 min. D) Amperometric measurement with capsule (different sensor) following repeated infill and purge of 3.6 ppm. E) Time-lapse photos of ingestible capsule showing feedback responsive triggering of an LED based on increasing $H_2S$ concentration above the proposed threshold value.

widely compatible with consumer electronic products. Known challenges of wireless communication for ingestible electronics include inefficient signal propagation within the GI tract, due to the high radio frequency (RF) signal attenuation in abdominal tissues ($\epsilon_r$ = 52.8),[78] high current consumption compared to sensing circuitry, and limited high-density battery chemistries that support high current consumption (≈10 mA) in a capsule form factor. To simulate the expected RF attenuation in vivo, the capsule was surrounded by 100 mm of ground meat (88% lean, 12% fat) on all sides (Figure S9, Supporting Information), and wireless signal attenuation testing was performed. The dielectric properties of the tissue analogue can be modified to precisely mimic the permittivity of human abdominal tissues using liquid phantoms or ballistic gel. A 100 mm thick layer of ground beef was utilized as a worst-case approximation to account for potential variations in dielectric constant between ground meat ($\epsilon$' = 45–55) and abdominal muscle.[79,80] This is because most signal attenuation occurs through abdominal muscle, which has an average thickness of only 5–10 mm.[81,82]

Previous studies have utilized similar tissue attenuation test methods or liquid phantoms as tissue analogues to benchmark Bluetooth signal propagation for medical use.[80,83–85] Further, capsule systems that utilize Bluetooth have been previously demonstrated.[74,86–88] In this work, the antenna gain of the BLE-MCU was restricted to +0 dB gain in order to evaluate Bluetooth with minimum power consumption, though transmission at +8 dB can be utilized sporadically to extend communication distance. The relative received signal strength (RSSI) between the device and a smartphone (Google Pixel 6, BLE) was recorded at various heights above the capsule. Validation of the unpackaged capsule electronics are shown in Figure S10 (Supporting Information). The separation distance from the phone was increased at 50 mm intervals until connection failure (Figure 4C). Figure 4D presents the averaged RSSI values through 100 mm of the tissue analogue. Reliable data transmission was maintained up to 720 mm, with a max RSSI of −99 dBm before disconnecting from the phone (antenna sensitivity is −100 dBm). An average RSSI value ($N$ = 30) was recorded at each height, showing an exponential decrease from the average baseline (100 mm separation) of −52 dBm in air taken as the system loss.

### 2.6. Electrochemical Measurement with Packaged $H_2S$ Gas-Sensing Capsule

**Figure** 5A shows the resulting amperometric measurement for the gas-sensing capsule with a bias voltage of −0.2 V (vs Ag), when tested under the same conditions as the benchtop sensors. A 14.6% $ppm^{-1}$ current response was observed, confirming that the capsule packaging, wireless communication, and mesoscale electronics does not impact sensor performance. A calibration curve, shown in Figure 5B, was generated by averaging the normalized current response from Nafion-Au $H_2S$ sensors ($N$ = 3) equipped to the gas-sensing capsule, where 100% represents 4.5 ppm $H_2S$. A linear current response (correlation coefficient $R^2$ = 0.9766) matched the saturation characteristics of the benchtop sensor characterization and a 0.13 ppm limit of detection (LOD) was calculated, indicating that the packaging did not have a negative impact on sensor response time or saturation characteristics. Benchtop testing confirmed $H_2S$ selectivity and sensitivity with the Au-Nafion sensor. However, in this controlled simulated environment the effects of the accumulation of proteins and lipids on the surface of the Teflon filter were not assessed, which could alter its diffusive properties leading to a deteriorated sensor response. Endoscopy capsules like the PillCam provide an outlook of the anticipated conditions, supporting the assumption that the sensor may be partially submerged during in vivo measurement throughout the GI tract.[89] The attached Teflon filter protects the Nafion membrane from direct exposure to acidic gastric fluids and alkaline bile salts (pH 7–8) in

the small intestine, a common concern with ingestible electronics, while also contributing to diffusivity through its pore size and hydrophobicity of the Teflon filter surface. Future efforts will focus on validating the gas-sensing capsule in solutions with acidic and slightly basic pH, as well as in simulated in vitro fluids, such as intestinal digesta or fistulated rumen. This evaluation will be conducted over the course of 12–24 h to evaluate sensor stability and the necessity for recalibration.[90]

### 2.7. Drift Characterization and Threshold Triggered Signaling

To demonstrate the utility of the gas-sensing capsule system to identify and respond to target gas concentrations, $H_2S$-driven feedback control was developed to trigger other downstream capsule functions. Previous sensor calibration curves were utilized to determine a suitable threshold concentration level and corresponding current response that represented an elevated $H_2S$ concentration. From the literature, trace $H_2S$ concentrations for patients with UC or SRB-related SIBO may exceed 30 ppm of intraluminal $H_2S$ in the colon, though in healthy patients has been shown to be substantially less (≈0.2 ppm).[19] Therefore, high sensitivity and selectivity for trace $H_2S$ levels in the large and small intestine is essential for correlating differences in healthy and diseased states. In a clinical setting sensor drift must be accounted for when determining a suitable threshold current value in real-time. Amperograms quantifying sensor drift were recorded to evaluate the stability of the Nafion-Au sensor (Figure 5C). To accomplish this, the system was placed in the test chamber and the $H_2S$ concentration was fixed at 3.6 ppm for 2 h. The sensor exhibited negligible drift for 30 min before the saturated current began to linearly drift back toward the sensor baseline at a rate of 0.1 nA $s^{-1}$ ($R^2 = 0.98$), Sensor drift is a known issue with Nafion sensors, and is possibly due to back-diffusion of water out of the Nafion membrane.[91,92] It is hypothesized that while electro-osmotic drag, H+ transport, and water transport contribute to the selective gas-diffusing properties of Nafion, water gradients within the membrane can also cause water to diffuse back out of the Nafion membrane after extended periods of activation. Membrane thickness, acid treatment, and substrate porosity significantly impact the prevalence of back diffusion, and therefore sensor drift.[93,94]

Considerations for progressively updating the threshold value will be required, either by introducing a linear correction factor to account for sensor drift exceeding acceptable 5% deviation in current response, or by delaying when the measurement occurs using pH targeting to localize specific sections of the small bowel amenable to the sensor's operational lifetime.[95–97] Threshold triggered signaling was demonstrated by placing the packaged capsule into the gas testing chamber and repeatedly modulating the $H_2S$ concentration between 0 and 3.6 ppm following saturation. Figure 5D shows the corresponding amperogram summarizing this implementation of the threshold value. Throughout the experiment the capsule was programmed to wireless alert the app when the current threshold value was surpassed. A video demonstrating when the $H_2S$ concentration level surpassed 3.0 ppm, indicated by a blue LED, was recorded with a phone (MovieS1, Supporting Information). The subsequent hydration, $H_2S$ infill, and $H_2S$ purge events are shown in Figure 5E, highlighting the potential of the system for deployment of complex monitoring and interventions in the GI tract.

To evaluate the $H_2S$ sensing platform in vivo, and ultimately for clinical use, several remaining challenges must be addressed, including system shelf-life, sensor stability, sensor drift, sterilization, and capsule miniaturization. With proper storage Nafion is expected to have a shelf life of up to 2 years, attributed to its chemical and mechanical durability. Future testing following an extended time in storage will be necessary to determine if the sensors require recalibration before ingestion. As calibration using a gas-testing chamber would be unrealistic in a clinical setting due to sterilizations concerns, special UV treatments could be performed to preserve Nafion membrane conductivity over time, potentially eliminating the need for recalibration.[98] The effects of such treatments and similar sterilization protocols on the semipermeable Teflon membrane filter require further investigation before adaptation of the sensing capsule for clinical use-cases. Additionally, the PDMS coating may be replaced by a robust biocompatible alternative, such as biocompatible epoxies or stereolithography (SLA) 3D-printed shells comprised of surgical guide resin (Formlabs), which has been demonstrated in similar capsule platforms that traverse the GI environment.[99,100]

While the introduced gas-sensing platform sufficiently validates the practicality of an amperometric ingestible capsule for $H_2S$ monitoring in a controlled environment, there are additional opportunities to improve the sensor's capabilities in terms of saturation limit and drift characteristics. The current sensor design saturates at 5.4 ppm, whereas exogenous concentrations of $H_2S$ can reach concentrations up to 30 ppm for patients with UC. Sensor saturation could be attributed to insufficient surface area of the thin-film Au electrodes, inadequate counter electrode size, or insufficient water uptake by the Nafion membrane. Further optimization of the Nafion membrane thickness and hydrating properties will allow tuning of this parameter, including adding feedback control to the gas-testing setup humidifying mechanism to correlate sensor response to humidity. Additionally, as sensor drift is influenced by Nafion membrane quality, substrate surface area, and substrate porosity, alternative strategies to reduce drift would involve reconfiguring the sensor to use a porous polyester track etch (PETE) membrane as both the substrate and semipermeable filter, utilizing a commercial Nafion 117 membrane or adjusting membrane pretreatment protocols to achieve a high-quality Nafion thin-film. The paradigm of integrating biosensor technologies and ingestible capsule systems offers desirable access, and is not only well positioned to enhance in vivo $H_2S$ monitoring capabilities but allow real-time detection of inflammatory biomarkers in the GI tract.

## 3. Conclusion

In summary, this work demonstrates the first wireless ingestible capsule system for monitoring patterns of $H_2S$ production in the GI tract. To enable $H_2S$ sensing in the humid GI environment, an Au electrochemical sensor was microfabricated and coated with a Nafion SEP pretreated with $H_2SO_4$. The sensor was characterized in a custom gas-testing setup with 100% humidity using a benchtop potentiostat, and exhibited a linear hydration-dependent electrochemical response to changes in $H_2S$ concentrations. $H_2S$ selectivity was confirmed using similar concentration ratios

(100-fold) of known interferent gases ($H_2$, $CO_2$, and $CH_4$) predominant in the GI tract. Front-end electronics were developed with Bluetooth wireless communication capabilities for portable amperometric measurement of $H_2S$, allowing modular integration the Au-Nafion sensor with the ingestible capsule platform. A capsule form factor ($14 \times 34$ mm$^2$) suitable for in vivo porcine studies was achieved using a PDMS polymer encapsulation strategy that successfully isolated the electronics from the surrounding moisture. Measuring signal attenuation of the ingestible capsule through media analogous to human tissues provided insights into the feasibility of Bluetooth Low Energy for in vivo applications. Further, analysis of sensor drift and threshold-based signaling demonstrated the utility of the capsule to perform continuous monitoring amenable for closed-loop operations. Future efforts will focus on correcting for sensor drift for prolonged operation throughout the entire GI transit, miniaturization of system components to achieve a smaller form factor, and integration of a pH sensor to support device localization, which together would support in vivo operation. The proposed platform is of great significance toward the study of transient gas dynamics in the GI tract, and may contribute to elucidating the etiology of inflammatory disease.

## 4. Experimental Section

*Fabrication of the Electrochemical $H_2S$ Sensor*: The electrochemical $H_2S$ sensor is comprised of three electrodes deposited on a flexible polyimide film (Kapton, 1 mil): a thin-film Au WE ( 4 mm diameter), Au CE, and a Ag RE. The concentric electrodes were designed using Autodesk AutoCAD (San Rafael, CA) and patterned via a series of paper shadow masks laser cut with a Glowforge Pro $CO_2$ laser cutter (GlowForge Inc., Seattle, WA). Prior to deposition, the mask was affixed to the polyimide substrate and baked in a furnace at 60 °C for 1 h to remove excess moisture. The exposed surface of the polyimide substrate was treated using an $O_2$ plasma cleaner (PX-250 Plasma Asher, March Instruments) with 4 SCCM of $O_2$ for 90 s at 150 W to improve thin-film adhesion. Metal layers of Cr/Au (20 nm/100 nm) were deposited using e-beam evaporation (Angstrom Engineering Inc., Cambridge, ON, Canada), followed by a separate deposition of Ag (300 nm) for the RE at deposition rates of 1.5, 2, and 2.5 Å s$^{-1}$, respectively. Sensors were cleaned with a combination of acetone, methanol, and isopropanol (AMI); rinsed thoroughly with DI water (>18.2 MΩ) from an E-pure Ultrapure Water Purification System (Thermo Scientific, Waltham, MA), and dried with $N_2$. To confine the Nafion membrane, an acrylic (10 mil) reservoir backed with 9495MP double-sided tape (3 M, Two Harbors, MN) was laser cut and attached above the sensor. The acrylic cutout (Ø = 12 mm) had a circular opening (Ø = 8 mm) positioned around the sensor electrodes, as well as three 1 mm ports aligned with the sensor contact pads. An identical acrylic layer (Ø = 12 mm), without the 8 mm cutout, was affixed to the back of the substrate to support the sensor assembly. To interface the sensor with the capsule electronics, a 20-AWG needle was used to make small perforations through the 1 mm openings aligned with each contact pad. Au header pins (3016-0-15-15-21-27-10-0, Mill-Max, Oyster Bay, NY) were inserted through the openings and secured with Ag epoxy (8330S, Digikey), and cured at 45 °C for 24 h. All sensors were examined for shorted electrical connections between the contact pins, cleaned with AMI, rinsed in DI water, and finally dried with $N_2$. This assembly strategy enables modular integration of the miniaturized $H_2S$ sensor within the ingestible capsule form factor.

*Formation and Pretreatment of Nafion Solid-State Polymer Electrolyte*: For the formation of the solid-state polymer electrolyte, a 5% w/v Nafion resin (EW, 1100 g eq$^{-1}$) mixture of lower aliphatic alcohols and water was purchased from Sigma-Aldrich (St. Louis, MO) and used as received. The Nafion dispersion (20 µL) was mixed in its original container for 60 s and then drop-cast onto the surface of the Au sensor. The sensors and a paper filter soaked in 80% diluted ethanol were placed in a small plastic Petri dish (30 mL) and sealed. The Petri dish was kept at room temperature for 24 h to slowly evaporate solvents from the Nafion resin, and then placed in a furnace for 1 h at 80 °C to completely remove the remaining solvents. Controlling the rate of solvent evaporation in ensures a uniform distribution of Nafion across the electrodes, minimizing the risks of cracks forming in the film.[54] The Nafion membranes were placed in a sealed humid container for 24 h to rehydrate. The films were functionalized by pretreatment with 0.1 M $H_2SO_4$ (50 µL) and resealed in the humid container for 48 h, allowing the acid to innervate the film. The sensor was then rinsed in DI water and stored in a humid chamber until use. Before use, a Teflon membrane (Ø = 6 mm, pore size: 5 µm) was lightly pressed into contact with the Nafion film and sealed. The Teflon membrane functions as a gas-permeable, liquid-impermeable interface between the Nafion and the external environment, preventing sensor corrosion and fouling of the sensor.

*Design and Assembly of Capsule Electronics*: A double-sided flex-rigid PCB was designed using Autodesk EAGLE (San Rafael, CA) and consists of two six-layer circular FR-4 ceramic substrates (Ø = 12 mm) connected by a 15 mm long polyimide flex connecting region with embedded copper traces (Sierra Circuits, Sunnyvale, CA) as shown in Figure S5A (Supporting Information). Several COTS components were incorporated into the design: 1) an electrochemical AFE, AD5941 (Analog Devices, Wilmington, MA), to excite the electrochemical sensor and record resulting current values using an onboard ADC and FRAM, 2) a BLE-MCU, BGM13S (Silicon Labs, Austin, TX), and external 2.45 GHz ceramic chip antenna, WLA.01 (Taoglas, San Diego, CA), for wireless data acquisition (signal power: 0 − +18 dBm) and energy management, and 3) a 3.3 V voltage regulator, TPS610981 (Texas Instruments, Dallas, TX), to maintain a constant operating voltage across all components (Figure S5C, Supporting Information). The system is powered by a 3.0 V, 160 mA h Li-$MnO_2$ coin-cell battery, 2L76 (Energizer, St. Louis, MO), featuring a high capacity-to-size ratio. Battery connections were made using 30 AWG insulated copper wires soldered to the (+) and (−) terminal of the battery. A nickel cap was spot welded to the (+) side of the coin-cell to facilitate the solder joint and avoid damaging the battery. The 30 AWG wires were guided through a 3D-printed spacer and connected to the corresponding power pins via Au pin receptacle. Additionally, a 15 AT magnetic reed switch, HSR-502RT (Hermetic Switch Inc, Chickasha, OK), is placed between the (+) battery terminal and the voltage regulator allowing the electronics to be turned on and off depending on the capsule's proximity to an external magnetic field, eliminating power consumption when in storage. Finally, three 22-AWG Au pins (5 mm) were mounted to the PCB to align and mount the WE, CE, and RE electrodes from the $H_2S$ sensor. Only digital signals and power traces were routed between the two rigid substrates to minimize signal noise due to bending the embedded flex connector (bend radius: 1.2 mm).

*Molding of Capsule Electronics*: The flex-rigid PCB, 3D-printed spacer, and battery were encapsulated in PDMS (Sylgard 184, Dow, Midland, MI) at a 10:1 monomer to curing agent ratio and baked at 65 °C for 24 h prior to removal. For PDMS encapsulation of the electronics, custom molds were designed in Fusion 360 (Autodesk, San Rafael, CA) and, using fused filament fabrication (FFF), were 3D-printed from PLA filament with a Prusa MK3S+ 3D-printer (Prusa Research, Prague, Czech Republic). The mold incorporated four embedded neodymium magnets to turn off the capsule during curing. The electronics were removed from the mold achieving a $14 \times 34$ mm$^2$ cylindrical capsule. Second, excess PDMS was removed to expose the Au pin connectors for the WE, CE, and RE electrodes, facilitating the connection of the $H_2S$ sensor and molded capsule electronics. A PLA cap (Ø = 14 mm) with a 6 mm opening was 3D printed to cover the Teflon protected sensor and was thermally melded to the rim of the cap to prevent liquid from shorting the sensor while still allowing gas to diffuse from the external environment. Finally, a PLA cap was sealed to the PDMS capsule with a biocompatible epoxy.

*Gas Testing Setup*: The custom-made gas testing set-up, as shown in Figure S2 (Supporting Information), provides a humid environment for modulating various intraluminal gas species. To generate specific concentrations, nonflammable calibration tanks (Gasco, Huntington Beach, CA)

of $H_2S$ (50 ppm, $N_2$-diluted), $H_2$ (3%, $N_2$-diluted), $CO_2$ (99.99%), and $CH_4$ (2.5%, air-diluted) respectively, were vented into a plastic test chamber (2400 mL) until the desired concentration was reached. Gas flow was regulated at two constant flow rates: 0.2 SLPM (standard liter per minute) for $H_2S$ and 0.4 SLPM for all proposed interferent gases ($H_2$, $CO_2$, and $CH_4$). Table S1 (Supporting Information) provides infill parameters used to calculate specific gas concentrations (in ppm) using Equation (1). To return the chamber to an ambient baseline condition (air), an outlet valve was opened, and the chamber contents were removed using a vacuum pump. The required venting time to return the sensor to its baseline value was dependent on the gas concentration in the chamber, though purging for three 20 s pulses followed by a 15 s wait time was sufficient for all test values and preserved sensor lifetime. A Mega2560 Arduino development board (Adafruit, New York, NY) and serial monitor was used to remotely control the test setup. A highly humid test environment was maintained using a water vapor atomizer (vapor rate: 380 mL $h^{-1}$) for 1 min following each cycle of gas purging and venting, as high relative humidity is essential for a conductive Nafion membrane.

*Calculation of $H_2S$ and Interferent Gas Concentrations*: The concentration of gas in ppm was calculated according to Equation 1

$$\frac{C_{\text{Tank}}\left[\frac{\text{mg}}{L}\right] \cdot Q\left[\frac{L}{s}\right] \cdot t_{\text{in}}\ [s]}{V_{\text{Cont}}} = \text{ppm} \tag{1}$$

where $V_{\text{Cont}}$ denotes the container volume, $C_{\text{Tank}}$, is the concentration of the gas calibration tank, $Q$ is the flow rate of the calibration gas, and $t_{\text{in}}$ is the infill time required to achieve specific gas concentrations. The volume of the container (2400 ± 30 mL) includes the volumetric sections of the test chamber and attached tubing. The initial ambient composition of the chamber is taken as air (79% $N_2$ and 21% $O_2$) at atmospheric pressure. $N_2$-diluted $H_2S$ is introduced into the container at 0.2 SLPM, or 0.0033 L $s^{-1}$, for 65 s. Interferent was added into the container at 0.4 SLPM, or 0.0067 L $s^{-1}$, for 6 s.

*Statistical Analysis*: Data were presented as mean ± standard deviation (SD). For gas sensing experiments, a sample size ($N = 3$) corresponds to the measurement of unique sensors, while for wireless attenuation testing, the number of replications ($N = 60$) refers to repeated measurements over time. Raw data collected from $H_2S$ sensors and the capsule platform represents an output current response, including a 10 min "warm-up time" to achieve a stable baseline current before the introduction of reactive gases. Data points recorded prior to the established "warm-up time" were excluded as outliers and not used in the evaluation of the sensor response. The remaining data points, after the "warm-up time," were analyzed using MATLAB to determine the current response following a 3 min "wait-time" after a gas was introduced. Peak current values were normalized to the highest linear concentration achieved (4.5 ppm) for both calibration and selectivity evaluation. No statistical methods were used to assess significant differences.

## Supporting Information

Supporting Information is available from the Wiley Online Library or from the author.

## Acknowledgements

This work was supported by the National Science Foundation ECCS Program under Award No.1939236. The authors thanked the technical support from TerrapinWorks and the Nanocenter FabLab at the University of Maryland. The authors also acknowledged support from the Clark Mid-Career Doctoral Fellows Program.

## Conflict of Interest

The authors declare no conflict of interest.

## Data Availability Statement

The data that support the findings of this study are available from the corresponding author upon reasonable request.

## Keywords

amperometry, gastrointestinal tract, hydrogen sulfide, Nafion, wireless ingestible capsule

Received: August 30, 2023
Revised: November 20, 2023
Published online: December 10, 2023

[1] M. J. Bull, N. T. Plummer, *Integr. Med.* **2014**, *13*, 17.
[2] R. Hills, B. Pontefract, H. Mishcon, C. Black, S. Sutton, C. Theberge, *Nutrients* **2019**, *11*, 1613.
[3] M. Rebersek, *BMC Cancer* **2021**, *21*, 1325.
[4] K. Dabke, G. Hendrick, S. Devkota, *J. Clin. Invest.* **2019**, *129*, 4050.
[5] J.-F. Leblanc, J. P. Segal, L. M. De Campos Braz, A. L. Hart, *Nutrients* **2021**, *13*, 1780.
[6] Y. R. Yu, J. R Rodriguez, *Semin. Pediatr. Surg.* **2017**, *26*, 349.
[7] N. de Bortoli, S. Tolone, M. Frazzoni, I. Martinucci, G. Sgherri, E. Albano, L. Ceccarelli, C. Stasi, M. Bellini, V. Savarino, E. V. Savarino, S. Marchi, *Ann. Gastroenterol.* **2018**, *31*, 639.
[8] L. A. Beardslee, G. E. Banis, S. Chu, S. Liu, A. A. Chapin, J. M. Stine, P. J. Pasricha, R. Ghodssi, *ACS Sens.* **2020**, *5*, 891.
[9] K. Kalantar-Zadeh, K. J. Berean, R. E. Burgell, J. G. Muir, P. R. Gibson, *Nat. Rev. Gastroenterol. Hepatol.* **2019**, *16*, 733.
[10] A. Rezaie, M. Buresi, A. Lembo, H. Lin, R. Mccallum, S. Rao, M. Schmulson, M. Valdovinos, S. Zakko, M. Pimentel, *Am. J. Gastroenterol.* **2017**, *112*, 775.
[11] C. De Geyter, K. Van De Maele, B. Hauser, Y. Vandenplas, *Nutrients* **2021**, *13*, 3261.
[12] J. L. Wallace, J.-P. Motta, A. G. Buret, *Am. J. Physiol. – Gastrointest. Liver Physiol.* **2017**, *314*, G143.
[13] D. J. Polhemus, D. J. Lefer, *Circ. Res.* **2014**, *114*, 730.
[14] F. Blachier, M. Andriamihaja, P. Larraufie, E. Ahn, A. Lan, E. Kim, *Am. J. Physiol. – Gastrointest. Liver Physiol.* **2020**, *320*, G125.
[15] J. Furne, A. Saeed, M. D. Levitt, *Am. J. Physiol. Regul. Integr. Comp. Physiol.* **2008**, *295*, R1479.
[16] H. Ding, J. Chang, F. He, S. Gai, P. Yang, *Adv. Healthcare Mater.* **2022**, *11*, 2101984.
[17] A. G. Buret, T. Allain, J.-P. Motta, J. L. Wallace, *Antioxid. Redox. Signal.* **2021**, *36*, 211.
[18] A. Birg, S. Hu, H. C. Lin, *JGH Open* **2019**, *3*, 228.
[19] S. Singh, H. Lin, *Microorganisms* **2015**, *3*, 866.
[20] P. Rose, P. K. Moore, M. Whiteman, C. Kirk, Y.-Z. Zhu, *Antioxid. Redox. Signal.* **2021**, *34*, 1378.
[21] K. Kalantar-Zadeh, K. J. Berean, N. Ha, A. F. Chrimes, K. Xu, D. Grando, J. Z. Ou, N. Pillai, J. L. Campbell, R. Brkljaca, K. M. Taylor, R. E. Burgell, C. K. Yao, S. A. Ward, C. S. Mcsweeney, J. G. Muir, P. R. Gibson, *Nat. Electron.* **2018**, *1*, 79.
[22] J. Z. Ou, C. K. Yao, A. Rotbart, J. G. Muir, P. R. Gibson, K. Kalantar-Zadeh, *Trends Biotechnol.* **2015**, *33*, 208.
[23] J. Z. Ou, J. J. Cottrell, N. Ha, N. Pillai, C. K. Yao, K. J. Berean, S. A. Ward, D. Grando, J. G. Muir, C. J. Harrison, U. Wijesiriwardana, F. R. Dunshea, P. R. Gibson, K. Kalantar-Zadeh, *Sci. Rep.* **2016**, *6*, 33387.
[24] K. J. Berean, N. Ha, J. Z. Ou, A. F. Chrimes, D. Grando, C. K. Yao, J. G. Muir, S. A. Ward, R. E. Burgell, P. R. Gibson, K. Kalantar-Zadeh, *Aliment. Pharmacol. Ther.* **2018**, *48*, 646.

[25] M. E. Inda, M. Jimenez, Q. Liu, N. V Phan, J. Ahn, C. Steiger, A. Wentworth, A. Riaz, T. Zirtiloglu, K. Wong, K. Ishida, N. Fabian, J. Jenkins, J. Kuosmanen, W. Madani, R. McNally, Y. Lai, A. Hayward, M. Mimee, P. N, A. P. Chandrakasan, G. TraversoS, R. T. Yazicigil, T. K. Lu, **2022**, pp. 17, https://doi.org/10.1101/2022.02.16.480562.
[26] K. Kalantar-Zadeh, N. Ha, J. Z. Ou, K. J. Berean, *ACS Sens.* **2017**, *2*, 468.
[27] C. M. Caffrey, K. Twomey, V. I. Ogurtsov, *Sens. Actuators, B* **2015**, *218*, 8.
[28] S. Gopalakrishnan, R. Thomas, S. Sedaghat, A. Krishnakumar, S. Khan, T. Meyer, H. Ajieren, S. Nejati, J. Wang, M. S. Verma, P. Irazoqui, R. Rahimi, *Biosens. Bioelectron. X* **2023**, *14*, 100380.
[29] H. Huang, C. Ehmke, C. Steiger, I. Ballinger, M. Jimenez, N. Phan, H. Sun, K. Ishida, J. Kuosmanen, J. Jenkins, J. Korzenik, A. Hayward, G. Traverso, in 2022 *44th Annual International Conference of the IEEE Engineering in Medicine & Biology Society (EMBC)*, IEEE, New York **2022**, pp. 2491–2494.
[30] K. H. Cha, X. Wang, M. E. Meyerhoff, *Appl. Mater. Today* **2017**, *9*, 589.
[31] Y. Deng, H. Qi, Y. Ma, S. Liu, M. Zhao, Z. Guo, Y. Jie, R. Zheng, J. Jing, K. Chen, H. Ding, G. Lv, K. Zhang, R. Li, H. Cheng, L. Zhao, X. Sheng, M. Zhang, L. Yin, *Proc. Natl. Acad. Sci. USA* **2022**, *119*, e2208060119.
[32] G. Barandun, L. Gonzalez-Macia, H. S. Lee, C. Dincer, F. Güder, *ACS Sens.* **2022**, *7*, 2804.
[33] J. M. Stine, S. Botasini, L. A. Beardslee, J. A. Levy, R. Ghodssi, in *Hilton Head Workshop 2022: A Solid-State, Sensors, Actuators, and Microsystems Workshop*, Hilton Head, SC, xx xx **2022**, pp. 81-84
[34] S. Mubeen, T. Zhang, N. Chartuprayoon, Y. Rheem, A. Mulchandani, N V. Myung, M A. Deshusses, *Anal. Chem.* **2010**, *82*, 250.
[35] C. Duc, M.-L. Boukhenane, J.-L. Wojkiewicz, N. Redon, *Front. Mater.* **2020**, 7.
[36] E. Llobet, J. Brunet, A. Pauly, A. Ndiaye, C. Varenne, *Sensors* **2017**, *17*, 391.
[37] E. Mutuyemungu, M. Singh, S. Liu, D. J. Rose, *J. Funct. Foods* **2023**, *100*, 105367.
[38] D. L. Kokkin, R. Zhang, T. C. Steimle, I. A. Wyse, B. W. Pearlman, T. D. Varberg, *J. Phys. Chem. A* **2015**, *119*, 11659.
[39] S. Mubeen, T. Zhang, N. Chartuprayoon, Y. Rheem, A. Mulchandani, N. V. Myung, M. A. Deshusses, *Anal. Chem.* **2010**, *82*, 250.
[40] H. Azher, C. A. Scholes, G. W. Stevens, S. E. Kentish, *J. Membr. Sci.* **2014**, *459*, 104.
[41] S. Sengupta, A. V. Lyulin, *J. Phys. Chem. B* **2019**, *123*, 6882.
[42] M. Mukaddam, E. Litwiller, I. Pinnau, *Macromolecules* **2016**, *49*, 280.
[43] A. Vishnyakov, R. Mao, M.-T. Lee, A. V. Neimark, *J. Chem. Phys.* **2018**, *148*, 24108.
[44] R. Devanathan, A. Venkatnathan, R. Rousseau, M. Dupuis, T. Frigato, W. Gu, V. Helms, *J. Phys. Chem. B* **2010**, *114*, 13681.
[45] S. Kim, K. No, S. Hong, *ChemComm* **2016**, *52*, 831.
[46] S. J. Peighambardoust, S. Rowshanzamir, M. Amjadi, *Int. J. Hydrogen Energy* **2010**, *35*, 9349.
[47] A. Pudi, M. Rezaei, V. Signorini, M. P. Andersson, M. G. Baschetti, S. S. Mansouri, *Sep. Purif. Technol.* **2022**, *298*, 121448.
[48] M. J. Cheah, I G. Kevrekidis, J. Benziger, *J. Phys. Chem. B* **2011**, *115*, 10239.
[49] T. Colinart, S. Didierjean, O. Lottin, G. Maranzana, C. Moyne, *J. Electrochem. Soc.* **2008**, *155*, B244.
[50] A. Z. Peng, A. Morin, P. Huguet, Y. Lanteri, S. Deabate, *Phys. Chem. Chem. Phys.* **2014**, *16*, 20941.
[51] M. A. Modestino, D. K. Paul, S. Dishari, S. A. Petrina, F. I. Allen, M. A. Hickner, K. Karan, R. A. Segalman, A. Z. Weber, *Macromolecules* **2013**, *46*, 867.
[52] S. C. Decaluwe, A. M. Baker, P. Bhargava, J. E. Fischer, J. A. Dura, *Nano Energy* **2018**, *46*, 91.
[53] C. S. Spiegel, *Designing and Building Fuel Cells*, McGraw-Hill Professional, New York **2007**.
[54] E. Passalacqua, R. Pedicini, A. Carbone, I. Gatto, F. Matera, A. Patti, A. Saccà, *Materials* **2020**, *13*, 5254.
[55] S. Pujiastuti, H. Onggo, *AIP Conf. Proc.* **2016**, *1711*, 60006.
[56] R. Kuwertz, C. Kirstein, T. Turek, U. Kunz, *J. Membr. Sci.* **2016**, *500*, 225.
[57] J. P. Popić, D. M. Dražić, *Electrochim. Acta* **2004**, *49*, 4877.
[58] M. Seifert, E. Brachmann, G. Rane, S. Menzel, T. Gemming, *Materials* **2017**, *10*, 54.
[59] J. Ramkumar, B. Venkataramani, *Alkali Metal Ion-Proton Exchange Equilibria and Water Sorption Studies on Nafon 117 Membrane and Dowex 50 W Exchange Resins: Effect of Long Storage or Aging* (BARC—2004/E/026), India, **2004**.
[60] S. F. Burlatsky, M. Gummalla, J. O'neill, V. V. Atrazhev, A. N. Varyukhin, D. V. Dmitriev, N. S. Erikhman, *J. Power Sources* **2012**, *215*, 135.
[61] U. Laforenza, *Mol. Aspects Med.* **2012**, *33*, 642.
[62] C. Steiger, A. Abramson, P. Nadeau, A. P. Chandrakasan, R. Langer, G. Traverso, *Nat. Rev. Mater.* **2018**, *4*, 83.
[63] S. Sarker, B. Wankum, T. Perey, M. M. Mau, J. Shimizu, R. Jones, B. Terry, *IEEE Trans. Biomed. Eng.* **2022**, *69*, 1870.
[64] K. Chen, L. Yan, Y. Sheng, Y. Ma, L. Qu, Y. Zhao, *ACS Nano* **2022**, *16*, 15261.
[65] L. J. Henze, N. J. Koehl, H. Bennett-Lenane, R. Holm, M. Grimm, F. Schneider, W. Weitschies, M. Koziolek, B. T. Griffin, *Eur. J. Pharm. Sci.* **2021**, *156*, 105627.
[66] J. H. Lee, G. Traverso, D. Ibarra-Zarate, D. S. Boning, B. W. Anthony, *J. Med. Device* **2020**, *14*, 021005.
[67] B. Orsini, S. Busechian, P. Faraoni, S. Burchielli, G. Maggi, F. Rogai, A. Gnerucci, P. Tortoli, S. Milani, C. Treghini, A. Dell'accio, G. Romano, F. Rueca, F. Fusi, *Photochem. Photobiol. Sci.* **2022**, *22*, 535.
[68] K. F. Schuster, C. C. Thompson, M. Ryou, *Clin. Endosc.* **2023**, https://doi.org/10.5946/ce.2022.293.
[69] S. S. Srinivasan, A. Alshareef, A. V. Hwang, Z. Kang, J. Kuosmanen, K. Ishida, J. Jenkins, S. Liu, W. A. M. Madani, J. Lennerz, A. Hayward, J. Morimoto, N. Fitzgerald, R. Langer, G. Traverso, *Sci. Robot.* **2022**, *7*, eabp9066.
[70] A. Abramson, E. Caffarel-Salvador, M. Khang, D. Dellal, D. Silverstein, Y. Gao, M. R. Frederiksen, A. Vegge, F. Hubálek, J. J. Water, A V. Friderichsen, J. Fels, R. K. Kirk, C. Cleveland, J. Collins, S. Tamang, A. Hayward, T. Landh, S T. Buckley, N. Roxhed, U. Rahbek, R. Langer, G. Traverso, *Science* **2019**, *363*, 611.
[71] S. H. Lee, J. Lee, Y. J. Yoon, S. Park, C. Cheon, K. Kim, S. Nam, *IEEE Trans. Biomed. Eng.* **2011**, *58*, 1734.
[72] A. Abid, J. M. O'brien, T. Bensel, C. Cleveland, L. Booth, B. R. Smith, R. Langer, G. Traverso, *Sci. Rep.* **2017**, *7*, 46745.
[73] V. Iacovacci, I. Tamadon, E. F. Kauffmann, S. Pane, V. Simoni, L. Marziale, M. Aragona, L. Cobuccio, M. Chiarugi, P. Dario, S. Del Prato, L. Ricotti, F. Vistoli, A. Menciassi, *Sci. Robot* **2021**, *6*, eabh3328.
[74] Y. L. Kong, X. Zou, C. A. Mccandler, A. R. Kirtane, S. Ning, J. Zhou, A. Abid, M. Jafari, J. Rogner, D. Minahan, J. E. Collins, S. Mcdonnell, C. Cleveland, T. Bensel, S. Tamang, G. Arrick, A. Gimbel, T. Hua, U. Ghosh, V. Soares, N. Wang, A. Wahane, A. Hayward, S. Zhang, B. R. Smith, R. Langer, G. Traverso, *Adv. Mater. Technol.* **2019**, *4*, 1800490.
[75] I. Miranda, A. Souza, P. Sousa, J. Ribeiro, E. M. S. Castanheira, R. Lima, G. Minas, *J. Funct. Biomater.* **2022**, *13*, 2.
[76] O. Ojuroye, R. Torah, S. Beeby, *Microsyst. Technol.* **2022**, *28*, 1467.
[77] M. Mimee, P. Nadeau, A. Hayward, S. Carim, S. Flanagan, L. Jerger, J. Collins, S. Mcdonnell, R. Swartwout, R. J. Citorik, V. Bulovic, R. Langer, G. Traverso, A. P. Chandrakasan, T. K. Lu, *Science* **2018**, *360*, 915.

[78] M. K. Magill, G. A. Conway, W. G. Scanlon, in *2015 Loughborough Antennas & Propagation Conference (LAPC)*, IEEE, New York **2015**, pp. 1–4.
[79] H. Chu, P.-J. Wang, X.-H. Zhu, H. Hong, *IEEE Access* **2019**, *7*, 35231.
[80] M. J. Christoe, J. Yuan, A. Michael, K. Kalantar-Zadeh, *IEEE Access* **2021**, *9*, 85144.
[81] A. Ido, Y. Nakayama, K. Ishii, M. Iemitsu, K. Sato, M. Fujimoto, T. Kurihara, T. Hamaoka, N. Satoh-Asahara, K. Sanada, *PLoS One* **2015**, *10*, e0143858.
[82] N. Tahan, K. Khademi-Kalantari, M. A. Mohseni-Bandpei, S. Mikaili, A. A. Baghban, S. Jaberzadeh, *J. Physiol. Anthropol.* **2016**, *35*, 17.
[83] F. Merli, L. Bolomey, J.-F. Zurcher, G. Corradini, E. Meurville, A. Skrivervik, *IEEE Trans. Antennas Propag.* **2011**, *59*, 3544.
[84] M. Suzan Miah, A. N. Khan, C. Icheln, K. Haneda, K.-I. Takizawa, *IEEE Trans. Antennas Propag.* **2019**, *67*, 2687.
[85] B. Biswas, A. Karmakar, V. Chandra, *IET Microw. Antennas Propag.* **2020**, *14*, 293.
[86] J. M. Stine, L. A. Beardslee, S. Chu, S. Liu, D. Motabar, W. E. Bentley, R. Ghodssi, *J. Microelectromech. Syst.* **2020**, *29*, 713.
[87] A. Sahafi, Y. Wang, C. L. M. Rasmussen, P. Bollen, G. Baatrup, V. Blanes-Vidal, J. Herp, E. S. Nadimi, *Sci. Rep.* **2022**, *12*, 13723.
[88] B. Hou, L. Yi, D. Hu, Z. Luo, D. Gao, C. Li, B. Xing, J.-W. Wang, C. N. Lee, R. Zhang, Z. Sheng, B. Zhou, X. Liu, *Nat. Biomed. Eng.* **2023**, *7*, 1242.
[89] B. Akpunonu, J. Hummell, J. D. Akpunonu, S. Ud Din, *Cleve Clin. J. Med.* **2022**, *89*, 200.
[90] U. Hoss, E. S. Budiman, *Diabetes Technol. Ther.* **2017**, *19*, S.
[91] T. A. Zawodzinski, C. Derouin, S. Radzinski, R. J. Sherman, V. T. Smith, T. E. Springer, S. Gottesfeld, *J. Electrochem. Soc.* **1993**, *140*, 1041.
[92] S. Paul Shylendra, M. Wajrak, K. Alameh, *Sensors* **2023**, *23*, 2331.
[93] A. Chouhan, B. Bahar, A. K. Prasad, *Int. J. Hydrogen Energy* **2020**, *45*, 10991.
[94] S. Jang, Y. S. Kang, D. Kim, S. Park, C. Seol, S. Lee, S. M. Kim, S. J. Yoo, *Adv. Mater.* **2023**, *35*, 2204902.
[95] G. E. Banis, L. A. Beardslee, J. M. Stine, R. M. Sathyam, R. Ghodssi, *J. Microelectromech. Syst.* **2019**, *28*, 219.
[96] G. E. Banis, L. A. Beardslee, J. M. Stine, R. M. Sathyam, R. Ghodssi, *Lab Chip* **2020**, *20*, 2020.
[97] M. A. Straker, J. A. Levy, J. M. Stine, V. Borbash, L. A. Beardslee, R. Ghodssi, *Microsyst. Nanoeng.* **2023**, *9*, 61.
[98] S. Shi, T. J. Dursch, C. Blake, R. Mukundan, R. L. Borup, A. Z. Weber, A. Kusoglu, *J. Polym. Sci. B: Polym. Phys.* **2016**, *54*, 570.
[99] H. Rezaei Nejad, B. C. M. Oliveira, A. Sadeqi, A. Dehkharghani, I. Kondova, J. A. M. Langermans, J. S. Guasto, S. Tzipori, G. Widmer, S. R. Sonkusale, *Adv. Intell. Syst.* **2019**, *1*, 1900053.
[100] E. De La Paz, N. H. Maganti, A. Trifonov, I. Jeerapan, K. Mahato, L. Yin, T. Sonsa-Ard, N. Ma, W. Jung, R. Burns, A. Zarrinpar, J. Wang, P. P. Mercier, *Nat. Commun.* **2022**, *13*, 7405.